

© 2015. Published by The Company of Biologists Ltd.

This is an Open Access article distributed under the terms of the Creative Commons Attribution License (<http://creativecommons.org/licenses/by/3.0>), which permits unrestricted use, distribution and reproduction in any medium provided that the original work is properly attributed.

## Localization-based imaging of malarial antigens during red cell entry reaffirms role for AMA1 but not MTRAP in invasion

David T. Riglar<sup>1,2,\*</sup>, Lachlan Whitehead<sup>1,2</sup>, Alan. F. Cowman<sup>1,2</sup>, Kelly L. Rogers<sup>1,2</sup> and Jake Baum<sup>3</sup>.

<sup>1</sup> The Walter and Eliza Hall Institute of Medical Research, Melbourne, Australia.

<sup>2</sup> Department of Medical Biology, University of Melbourne, Australia.

<sup>3</sup> Department of Life Sciences, Imperial College, London, SW7 2AZ, United Kingdom.

**KEYWORDS:** *Plasmodium*; merozoite; erythrocyte invasion; tight junction; deconvolution

### Correspondence to:

Jake Baum

Department of Life Sciences

Imperial College, London, SW7 2AZ

United Kingdom

Email: [jake.baum@imperial.ac.uk](mailto:jake.baum@imperial.ac.uk)

\*Present address: Department of Systems Biology, Harvard Medical School, Boston, USA.

## ABSTRACT

Microscopy-based localisation of proteins during malaria parasite invasion of the erythrocyte is widely used for tentative assignment of protein function. To date, however, imaging has been limited by the rarity of invasion events and poor resolution available, given micron size of the parasite, which leads to a lack of quantitative measures for definitive localisation. Here, using computational image analysis we have attempted to assign relative protein localisation during invasion using wide-field deconvolution microscopy. By incorporating three-dimensional information we present a detailed assessment of known parasite effectors predicted to function during entry but as yet untested or for which data is equivocal. Our method, longitudinal intensity profiling, resolves confusion surrounding localisation of apical membrane antigen (AMA1) at the merozoite-erythrocyte junction and predicts that the merozoite thrombospondin related anonymous protein (MTRAP) is unlikely to play a direct role in the mechanics of entry, an observation supported with additional biochemical evidence. This approach sets a benchmark for imaging of complex micron-scale events and cautions against simplistic interpretations of small numbers of representative images for assignment of protein function or prioritisation of candidates as therapeutic targets.

## INTRODUCTION

In the biological sciences, microscopy is generally used to translate information contained within a tissue or cell specimen into a more useful format, such as a processed digital image. While the degradation of data due to imaging and image analysis is generally well understood and accepted (North, 2006) the loss of information resulting from image selection and presentation is frequently ignored. Certainly one of the key strengths of high-throughput automated and quantitative imaging studies is that they circumvent these issues and allow presentation of large quantities of data without interference from direct bias (Zhan et al., 2015). Many imaging workflows, however, are not amenable to such imaging approaches. Imaging of *Plasmodium falciparum* merozoites caught during invasion of the human erythrocyte (Boyle et al., 2010b; Riglar et al., 2011) is one such example.

The blood stage merozoite is one of the smallest eukaryotic cells. Responsible for setting up the blood stages of infection (and therefore for the entirety of malaria disease pathology (White et al., 2014)), each merozoite measures only 1-2 $\mu$ m in length with a cellular role almost entirely geared towards erythrocyte invasion (Bannister and Mitchell, 2009). The process of invasion (reviewed in (Cowman et al., 2012)) commences with a weak attachment between multiple merozoite surface proteins (MSPs) and the erythrocyte. This initial contact between the merozoite and erythrocyte surfaces induces physical changes in the target erythrocyte membrane, possibly due to reorganization of the erythrocyte cytoskeleton (Zuccala and Baum, 2011). This is then followed by reorientation of the merozoite to its apical pole, bringing the core invasion machinery at the parasite's apex in contact with the erythrocyte membrane (Dvorak et al., 1975). The apical complex at this pole contains specialized organelles termed the micronemes and rhoptries that secrete protein and lipids during invasion (Cowman et al., 2012). Following an, as yet, unknown trigger signaling commitment to invasion, the merozoite becomes irreversibly attached to the erythrocyte and initiates a cascade of cellular and molecular events that guide the invasion process through to completion (Hanssen et al., 2013; Riglar et al., 2011; Weiss et al., 2015). Chief among these interactions is the establishment of the tight or moving junction (Aikawa et al., 1978; Bannister et al., 1975) a molecular aperture in the red cell through which the parasite passes en route to infection. The junction, acting as the key organizing nexus for invasion, is thought to correspond to a key molecular interaction between two classes of parasite protein: the rhoptry neck proteins (RONs), that are embedded in or under the target erythrocyte membrane (though parasite derived); and a micronemal protein apical membrane antigen 1 (AMA1) which is present on the merozoite surface at the time of invasion (Riglar et al., 2011). Evidence from both *P. falciparum* and a closely related Apicomplexan parasite, *T. gondii*, demonstrates that AMA1 binds an extracellular loop of RON2 through a deep molecular interaction (Lamarque et al., 2011; Srinivasan et al., 2011; Tonkin et al., 2011; Tyler and Boothroyd, 2011). This link has led to the hypothesis that the tight junction is the point of traction for the merozoite (and *T. gondii* tachyzoite) during invasion, against which (either directly or indirectly) the forces of the internal parasite

actomyosin motor (or gliding motor) leverage to drive the parasite into the host cell (Angrisano et al., 2012; Bichet et al., 2014). The motor itself is housed in the outer pellicle of the merozoite and is formed between a short single-headed class XIV myosin interacting with dynamic, though poorly understood filaments of actin (Baum et al., 2006a). As invasion progresses, various merozoite surface proteins are differentially proteolytically cleaved from the surface (Bannister et al., 1975; Boyle et al., 2014; O'Donnell et al., 2006). In addition, a largely parasite-derived vacuole surrounding the invading merozoite is established, called the parasitophorous vacuolar membrane (PVM), thought to be composed of a combination of parasite and host cell lipids (Lingelbach and Joiner, 1998). Upon completion of invasion, the erythrocyte membrane and PVM seal and the tight junction disintegrates (Riglar et al., 2011; Riglar et al., 2013).

Once the events of invasion are initiated, the tight junction is one of the clearest reference points for determining the organisation of molecular events at the site of entry (Riglar et al., 2011; Zuccala et al., 2012). The absolute size of the junction, at around a micron in diameter, however, presents a significant challenge for assigning protein presence, absence or co-localisation with its small structure. To overcome this we have previously used wide-field deconvolution and three-dimensional structured illumination (3D SIM) 'super resolution' microscopy methods to observe three-dimensional distribution of protein labelling during merozoite invasion (Riglar et al., 2011; Zuccala et al., 2012). Even with these advances, analyses have most often been limited to the presentation of a small number of representative images. Given that significant variability between individual parasites is often seen (Zuccala et al., 2012), the presentation of low numbers of images combined with the size of the merozoite in comparison to microscopy resolution limits presents a major challenge when attempting to assign an absolute distribution of a protein through time.

Given these challenges we sought to adapt our methods for analysing images of invading merozoites (Boyle et al., 2010b; Riglar et al., 2011), developing a computational workflow towards a more quantitative and unbiased determination of protein distribution during the process of merozoite invasion. In particular we focussed on the longitudinal distribution of proteins with respect to the tight junction as the merozoite enters the erythrocyte and the variability shown across parasites.

## RESULTS

### *A workflow towards unbiased localisation of proteins at the merozoite-erythrocyte tight junction*

Recognising the need for a robust and reproducible means of localising proteins during the process of malaria parasite entry into the human erythrocyte (Fig. 1A), we developed a workflow (longitudinal intensity profiling) of image capture and processing to localise proteins to the merozoite-erythrocyte tight junction with respect to the junctional marker, *rho*protry neck protein (RON)-4 (see *Materials and Methods* and Fig. 1B). While variations in extent of invasion still prohibit wholesale quantification across multiple parasites (save perhaps for the region directly within the RON4 tight junction ring), the realignment provided by rotation and skew correcting steps in this workflow should allow unprecedented reliability in evaluating large numbers of merozoite invasion events. As a first test to explore the reproducibility and utility of this workflow, invading merozoites were labelled using rabbit antiserum and mouse monoclonal antibodies both raised against RON4 (Richard et al., 2010) (Fig. 1C, Fig S1A; total number of merozoites analysed,  $n=16$ ). A single, clear RON4 peak was present in almost every line profile, particularly using the monoclonal, confirming the successful re-alignment of data in the z-direction. Peak intensity in both channels was consistently found at the same point (e.g. Fig. 1C right panel, example parasites 4 and 11). As previously observed (Riglar et al., 2011), background fluorescence was noticeable in many samples labelled using rabbit RON4 antisera, both within the parasite and within the erythrocyte, visible as a higher normalised baseline labelling than that of the monoclonal and in common spurious minor peaks within intensity profiles (e.g. Fig. 1C right panel, example parasites 13 and 16). In all cases the intensity profile matched features that were visible within the 3D image stacks (*data not shown*) though these were not always apparent in individual slices, such as those depicted in the example merozoite figures displayed in the right panel. Of note, taking an individual invading merozoite through the analysis pipeline three separate times (Fig. 1D) gave very similar results (pairwise  $R^2$  values of linear regressions for correlations between corresponding values of normalised longitudinal intensity profiles between image pairs of 0.975, 0.930 and 0.932 respectively) suggesting the workflow is robust and provides a reliable means for assessing protein localisation during invasion. The initial results also supported the preferential use of the mouse RON4 monoclonal as a control label for the tight junction in further assays.

### *Analysis of AMA1 during invasion identifies the presence of masked epitopes in samples.*

Having established a reliable computational workflow for longitudinal intensity profiling, we next applied this method to a second key component of tight-junction dependent invasion, the apical membrane antigen 1 (AMA1) (Tyler et al., 2011). Whilst a large body of literature points to this protein playing a critical role at the tight junction recent publications have called into question this protein's essentiality during malaria parasite (*Plasmodium*) invasion (Bargieri et al., 2013; Yap et

al., 2014) as well as that of the related apicomplexan parasite *Toxoplasma gondii* (Bargieri et al., 2013; Lamarque et al., 2014). Some of this discussion has focussed on AMA1 localisation at the tight junction, for example its general absence from this site during *T. gondii* tachyzoite invasion of fibroblasts (Giovannini et al., 2011). Our own imaging of 20 invading *P. falciparum* merozoites co-labelled with RON4 monoclonal, demonstrated AMA1 very much present, and most often concentrating, at the tight junction during invasion (Riglar et al., 2011).

To re-address the population level variability of AMA1 localisation during *P. falciparum* merozoite invasion using longitudinal intensity profiling, invading merozoites were co-labelled with either the RON4 monoclonal (Richard et al., 2010) and rabbit AMA1 antiserum (Healer et al., 2002) or rabbit RON4 antiserum (Richard et al., 2010) with the well-characterised AMA1 1F9 monoclonal antibodies (Coley et al., 2001). Consistent with our previous results (Riglar et al., 2011), rabbit AMA1 antiserum labelled a portion of AMA1 localised directly within the RON4 annulus in all parasites imaged (Fig. 2A, Fig. S1B;  $n=19$ ). This junctional AMA1 population varied in its relative intensity compared to global AMA1 labelling, which regularly included apical and broad surface localisations. Importantly, however, even the lowest level of junctional AMA1 labelling was appreciably higher than background labelling levels (e.g. Fig. 2A, example 14).

In contrast to polyclonal labelling, AMA1 1F9 monoclonal antibodies showed a clear absence of signal within the RON4 demarked tight junction, evident as local minima in intensity profiles across the parasites imaged (Fig. 2B, Fig. S1C;  $n=17$ ). AMA1 1F9 antibodies bind the hydrophobic cleft of the AMA1 molecule (Coley et al., 2007), the same groove with which RON2 interacts (Lamarque et al., 2011; Tyler and Boothroyd, 2011). When viewed together, these results suggest that AMA1 is indeed present at the tight junction of invading *P. falciparum* merozoites, with micronemal and surface populations also regularly present, but that selection of immune-label is critical. The 1F9 epitope is clearly masked by interactions occurring at the tight junction, most likely with RON2, under the fixation and permeabilization conditions used. This likely explains the absence of labelling seen in previous studies with *T. gondii* as the result of epitope masking (Giovannini et al., 2011) and highlights the importance of using multiple antibodies to assign protein localisation, in particular polyclonal antibodies with multiple epitopes. Various attempts to expose masked epitopes, including heat, organic solvent based-permeabilization (e.g. methanol or acetone) and other detergents (e.g. saponin) were unsuccessful. This remains an important limitation for the imaging of invading *P. falciparum* merozoites using our current method.

#### *Actin and aldolase localise in a manner consistent with the motor model during merozoite invasion*

The current model for actomyosin motor involvement during invasion, whilst again the subject of various conflicting genetic deletion data (Andenmatten et al., 2013; Drewry and Sibley, 2015; Egarter et al., 2014), remains largely untested in *P. falciparum* merozoite invasion. We therefore

used the longitudinal intensity profiling workflow to systematically dissect the localisation of several key components of the parasite's actomyosin motor during merozoite invasion.

We have previously imaged merozoite actin during *P. falciparum* erythrocyte invasion (Angrisano et al., 2012; Riglar et al., 2011; Wong et al., 2011), showing a concentration of actin in a band at the parasite periphery, extending from the tight junction towards the rear of the parasite. Using 3D structured illumination microscopy (3D SIM), the concentration of actin at the tight junction appeared to be slightly posterior to the movement of the junction as the parasite invaded (Angrisano et al., 2012). Using the current workflow, actin labelling similarly showed a consistent peak of intensity in the approximate region of the tight junction (Fig. 3A, Fig. S1D;  $n=19$ ), varying in its position from distinctly behind the RON4 demarked tight junction (e.g. Fig. 3A, parasites 4 and 8) to overlapping with the junction (e.g. Fig. 3A, parasites 15 and 16). In almost all images analysed, actin fluorescence intensity was at least 50% of peak values at some position within the junction. Aligning the full range of parasites imaged demonstrated a tendency for parasites that are later in the invasion process to show higher levels of actin staining directly within the RON4 junction (Fig. 3A, parasites 12-19). The bias in later stages may be explained by the steeper curvature of the parasite at its apex. In addition,  $\pm 50\%$  of parasites imaged showed strong apical actin labelling. These observations, whilst inconclusive with respect to the precise junction-overlap and the possible cause for variable apical actin labelling, are consistent with the actomyosin traction force being at or directly adjacent to the tight junction in line with recent reports from *T. gondii* (Bichet et al., 2014).

The role of aldolase as a necessary link between motor force and the host cell has recently come under renewed scrutiny, seeming to be superfluous to motor activity (Shen and Sibley, 2014). Longitudinal intensity profiling of the distribution of aldolase in the invading merozoite showed strikingly similar features to that of actin (Fig. 3B, Fig. S1E;  $n=19$ ). Foremost, peak aldolase fluorescence was consistently found just rearward of the RON4 demarked tight junction (e.g. Fig. 3B, parasites 6 and 10) and in addition, aldolase fluorescence within the tight junction was regularly at least 50% of peak intensity levels. Of note, some parasites displayed a peripheral labelling pattern for aldolase (e.g. Fig. 3B, parasites 14 and 16) as has been described, albeit with conflicting evidence, in extracellular *T. gondii* previously (Pomel et al., 2008; Starnes et al., 2009). Combined, these data are consistent with aldolase being present at the site of motor activity and junction formation, irrespective of whether aldolase is a necessary link to the motor or a recruited component of the energy production machinery required for invasion.

#### *MTRAP localisation during invasion questions its proposed role in invasion.*

Under the current actomyosin motor model, filamentous actin links through to proteins of the thrombospondin related anonymous protein (TRAP) family that act as key traction mediators in both motility (gliding in sporozoites and ookinetes) and invasion (for a review see (Baum et al.,

2008)). In the case of the merozoite this is thought to utilise the stage-specific merozoite TRAP orthologue, MTRAP (Baum et al., 2006b). This family of proteins shares various features including the presence of adhesive extracellular domains that may assist in attachment to the host cell and thus act as a traction point during motility and invasion. In support of this model, MTRAP has recently been reported to interact with Semaphorin7A on the erythrocyte surface through its extra-parasitic thrombospondin repeat domains (Bartholdson et al., 2012). Given this putative role in transmitting traction force, a key prediction of the motor model would be that MTRAP should localise to the junction during invasion.

One challenge with assessment of MTRAP localisation during invasion is that it undergoes several processing events during maturation, resulting in cleavage of the extracellular TSR domain from the stub of cytoplasmic tail at or prior to invasion (Baum et al., 2006b). Towards assessing each component, we generated rabbit antisera against MTRAP's C-terminal tail and a rabbit monoclonal antibody against a peptide spanning an unstructured region in MTRAP's extracellular domain downstream of the TSR region, termed the mid domain (Fig. 4A). Combined with rabbit antisera generated against MTRAP's TSR domain (Baum et al., 2006b), these sera enabled labelling and distinction of the various MTRAP species (Fig. 4B), which along with RON4 by longitudinal intensity profiling demonstrated several significant insights into MTRAP biology (Fig. 5A-C, Fig. S2A-C).

MTRAP tail antisera consistently labelled the merozoite surface (e.g. Fig. 5A, parasites 3, 6 and 11, Fig. S2A;  $n=13$ ). Strong apical labelling was also regularly seen using this antiserum (e.g. Fig. 5A, parasite 6). Both distributions are consistent with MTRAP's micronemal localisation and release onto the merozoite surface during the invasion period (Baum et al., 2006b). Of note, however, MTRAP labelling intensity was often at a local minimum within the RON4 demarked tight junction. Labelling was also commonly absent in the region immediately towards the rear of the merozoite from the tight junction, the localisation where actin and aldolase also regularly concentrated. This latter observation could suggest either an absence of MTRAP within the tight junction zone, caused by either active or passive exclusion, the presence of epitope masking similar to that observed with AMA1 IF9 labelling (see above), or issues with general antibody accessibility within the junction region of the periplasmic space. To investigate this latter possibility we tested the IMC and PM anchored protein GAP45, which in developing merozoites shows a consistent labelling surrounding the parasite and would be expected to localise within the same periplasmic space as MTRAP's tail (Baum et al., 2006b). While GAP45 intensity commonly dropped slightly within the region of the tight junction, intensity was regularly well above 50% of its peak in this region (Fig. S3A;  $n=15$ ). Combined with the regular observation of fluorescence within the junction region of parasites labelled with actin and aldolase antisera, both periplasmic proteins, we concluded that antibody access to the inner face of the junction region is unlikely to be the sole cause of fluorescence minima in the region. It remains possible that the MTRAP tail may still experience epitope masking at the tight junction, since the polyclonal serum was raised against

only the short C-terminal tail peptide, which may have given rise to a markedly reduced repertoire of potential epitopes. Evidence for this limitation is seen when the endogenous MTRAP protein is tagged at its C-terminus, which renders the protein unrecognisable by this antiserum (Fig. 4B). Nonetheless, the balance of data presented here runs contrary to our expectations of MTRAP concentration solely at the junction.

Given our inability to make clear conclusion from investigation of MTRAP tail localisation, we next investigated the localisation of the MTRAP mid domain during invasion (Fig. 5B, Fig. S2B;  $n=27$ ). The MTRAP mid domain appeared to localise in a punctate or dappled fashion around the merozoite surface in addition to commonly strong apical fluorescence associated most likely with unreleased micronemes. Punctate background fluorescence was often visible within erythrocytes and manifested as high and variable baseline fluorescence in longitudinal intensity profiles, in particular at the front end (right hand side) of the profiles (e.g. Fig. 5B, parasites 11, 22, 26). Close inspection of intensity profiles, however, did highlight the presence of high intensity labelling just rearward of, and often directly within, the RON4 labelling tight junction in many parasites (e.g. Fig. 5B, parasites 11, 15, 22, 27) but not all (e.g. Fig. 5B, parasite 26). An explanation for the differences in restricted versus more diffuse localisation between the mid domain and tail antibodies respectively may be due to the predicted proteolytic cleavage and retention of the tail stub post-MTRAP function during invasion. To add further data to resolve this, we investigated the localisation of MTRAP's TSR domain (Fig. 5C, Fig. S2C;  $n=18$ ) the expected functional adhesive domain of the protein (Bartholdson et al., 2012). Labelling was most commonly found only at the apical tip of the parasite (e.g. Fig. 5C, parasites 4, 8) with small patches of fluorescence at times also present in distinct areas of the parasite periphery or internally within the merozoite (e.g. Fig. 5C, parasites 14, 2). These observations were confirmed in the longitudinal intensity profiles, which most commonly showed only a strong apical peak within the parasite at varying distances from the RON4 junction corresponding to individual parasite's progression through invasion. Strikingly, intensity was commonly almost completely absent within the zone of the tight junction and rarely present rearward from the junction. These results go entirely contrary to predictions given the presumed adhesive role of the MTRAP TSR domain and its demonstrated interaction with the erythrocyte surface receptor Semaphorin 7A (Bartholdson et al., 2012). Furthermore, given the polyclonal nature of MTRAP TSR antisera and the clear ability for antibodies to access the junction, as demonstrated by AMA1 polyclonal serum, we do not believe this is an issue of epitope masking.

### *Spatiotemporal analysis of MTRAP cleavage*

Given the surprising lack of mid-invasion surface labelling by MTRAP TSR, but the presence of labelling by MTRAP mid and tail domains, we wanted to investigate the spatiotemporal processing of MTRAP before and during invasion using a complementary approach towards final assessment

of its functional role in invasion. MTRAP has previously been shown to undergo processing within its extracellular domain by immuno-blot (Baum et al., 2006b). The protein also possesses an intramembrane rhomboid protease cleavage recognition site, which can be cleaved by PfRhom4 in a heterologous assay (Baker et al., 2006). Like other TRAP family proteins or invasion ligands, our current hypothesis suggests that MTRAP is shed from the merozoite surface during invasion (O'Donnell and Blackman, 2005). MTRAP's N-terminal TSR domain is found abundantly within culture supernatant in support of its cleavage and release post-invasion (Baum et al., 2006b).

Different MTRAP antibodies consistently recognised a distinct set of MTRAP fragments (Fig. 4B): MTRAP TSR antiserum labelled full length MTRAP, which runs on SDS-PAGE gels at ~75 kDa and the N-terminal fragment post-cleavage, which runs ~27 kDa; MTRAP mid antibodies also recognised full length MTRAP, along with two cleaved fragments running at approximately ~38 and 44 kDa; MTRAP tail antiserum recognised the same species as the mid domain antibodies, with the addition of a small band that ran at ~15 kDa – the cleaved tail stub, although the latter species was never detected in high abundance, perhaps suggestive of fast degradation rates or low percentage retention during SDS-PAGE and immuno-blot analysis. To investigate the cleavage of MTRAP during the lifecycle we performed a parasite developmental time course, harvesting tightly synchronised parasites either as <40 h, <42.5 h, <45 h post-invasion schizonts or following egress and reinvasion of a significant proportion of parasites (Fig. 6A, lanes 1-4). Immuno-blot analysis using rabbit MTRAP tail antiserum showed the progressive appearance of ~44 kDa cleavage products during schizogony (Fig. 6A, lanes 2-3), and of cleaved MTRAP tail in the ring-schizont mixed population (Fig. 6A, lane 4). The early appearance of ~44 kDa cleavage products in schizont samples was unexpected since it would indicate a separation of the N-terminal TSR domain from the remainder of MTRAP, a process previously presumed to occur during invasion in a shedding-type event.

There remained a possibility that the cleavage detected may derive from breakthrough or fast-growing parasites that had already undergone egress and invasion. To determine the dependency of cleavage on merozoite invasion and rupture, we treated parasites that had been synchronised simultaneously with those above, with either the carbohydrate heparin, which is an inhibitor of merozoite invasion (Boyle et al., 2010a), or the cysteine protease inhibitor trans-Epoxy succinyl-L-leucylamido(4-guanidino)butane (E64), which is an inhibitor of merozoite egress (Salmon et al., 2001). These parasites were allowed to grow and rupture in the presence of the respective drugs before being harvested simultaneously with mixed ring-schizont samples (Fig. 6A, lanes 5-6). Strikingly, the presence of all major MTRAP cleavage products in drug treated samples suggested that MTRAP cleavage occurred independently of both invasion and schizont rupture. While, it remains possible that MTRAP cleavage was occurring aberrantly from the surface of the heparin-inhibited merozoites that remained in the media (Fig. 6A, lane 6), only low levels of breakthrough invasion were seen following E64 treatment (*data not shown*) thus making it highly unlikely that a

similar degree of cleavage could be attributed to only those parasites escaping E64 inhibition (Fig. 6A, lane 5).

Given this unexpected early cleavage of MTRAP's N-terminal, TSR-containing domain from the rest of the protein, we further investigated processing using E64 and treatment with a combination of the protease inhibitors antipain and leupeptin, which together act to block egress (Wickham et al., 2003). As before, inhibition of egress was confirmed to have no effect on the cleavage of the TSR domain as measured by release of the ~27 kDa TSR fragment labelled using rabbit antiserum raised against the TSR domain and by the presence of the ~44 kDa MTRAP fragment labelled using rabbit antiserum raised against the C-terminal tail (Fig. 6B).

While our results suggested that cleavage could occur independently of invasion, contact with erythrocytes and even correct egress, we next wanted to investigate whether the model for shedding was still valid by determining whether cleavage occurred only after microneme release and exposure of MTRAP on the merozoite surface. Due to the difficulties with obtaining sufficient numbers of appropriately late schizonts for rigorous analysis, we synchronised parasites to a ~4hr window, treated late schizonts with E64 and allowed them to progress past their expected time of rupture. The resultant samples contained parasites ranging from late schizonts to the membrane-confined sacs of merozoites typical of E64 treatment. IFA of these parasites, following their fixation on glass slides using methanol, was used to co-label AMA1 and the different MTRAP antisera (Fig. 6C). E64 treated samples consistently showed evidence of microneme secretion occurring in later stage parasites. In many parasites, AMA1 labelling localised to the merozoite surface (Fig. 6C), although earlier stage schizonts that still showed the punctate fluorescence associated with unreleased micronemes were also present within the samples (Fig. 6C, top panels). Co-labelling with MTRAP tail (Fig. 6C, left hand panels) showed progressively increased labelling associated with the merozoite surface in parasites displaying partial and full AMA1 surface distribution respectively. Conversely, MTRAP mid (Fig. 6C, middle panels) and MTRAP TSR (Fig. 6C, right hand panels) both showed dispersed labelling in E64 treated schizonts and evidence of lowered labelling and dispersal of signal in parasites that appeared to have at-least partially burst from their surrounding membranes (Fig. 6C, bottom panels).

To relate these results to untreated parasites, we next imaged tightly synchronised schizonts co-labelled with AMA1 and MTRAP antibodies (Fig. 6D). While the vast majority of parasites in these samples showed no evidence of microneme secretion, a small percentage commonly showed evidence of partial AMA1 redistribution to the merozoite surface, indicative of microneme release beginning prior to egress from the schizont. This result is consistent with the timing of AMA1 secretion following reversible treatment of parasites with the PfPKG inhibitor, Compound 1 (C1) (Collins et al., 2013b). We did not observe any parasites showing complete AMA1 or any clear MTRAP redistribution to the merozoite surface, suggesting that this phenotype may be specific to parasites arrested from egress using E64. These results are therefore consistent with both MTRAP

TSR and mid domains being released from the merozoite surface following microneme secretion, but in a manner independent of invasion or egress from the schizont. It remains unclear whether MTRAP, like AMA1, is released onto the merozoite surface just prior to egress or if MTRAP and AMA1 reside in distinct populations of micronemes.

Finally, to investigate whether MTRAP cleavage could occur prior to microneme secretion, we arrested tightly synchronised parasites prior to microneme secretion using C1 (Fig. 7) (Collins et al., 2013b). Co-labelling between AMA1 and MTRAP antibodies confirmed that parasites treated in this manner retained only punctate localisations of both proteins, even in cases where merozoites appeared to have burst from the membranes surrounding the schizont (Fig. 7A). Immuno-blot analysis of saponin-lysed parasite samples was then undertaken to assess MTRAP's cleavage state (Fig. 7B). The successful activity of C1 was confirmed by immuno-blot, which showed cleavage of MSP1 to form the MSP1-42 cleavage in DMSO treated control parasites but not in parasites treated with 2.5  $\mu$ M C1. Surprisingly, despite the lack of microneme secretion, clear evidence of MTRAP cleavage to release the 27 kDa TSR-containing fragment recognised by antiserum raised against MTRAP TSR domain, and the ~44 kDa product labelled by antiserum raised against MTRAP's C-terminal tail (Fig. 7B). Similarly, AMA1 prodomain cleavage to form the 66 kDa product occurred independently of microneme secretion (Fig. 7B).

Taken together these results suggest that the TSR of MTRAP is cleaved from the remainder of the protein prior to secretion onto the merozoite surface (Fig. 7C). Thus, as uncovered via our imaging approach and followed up with biochemical and imaging assessment of MTRAP's distribution, these results strongly call into question our current MTRAP-dependent model for merozoite invasion.

## DISCUSSION

One of the critical challenges of fluorescence microscopy and its application to cellular biology is that of subjectivity. How do we assess the reliability of images, acquired with all the rigor possible (Waters and Wittmann, 2014) in the support or rejection of a hypothesis without bias? For single molecule imaging, there is already a large discipline of statistical approaches for assessing molecule distribution that can be used to rigorously test the localisation of different proteins (Sauer, 2013). For conventional imaging, however, whilst there is a general understanding that unbiased approaches are important there are few guidelines as to how many images are required or what analytical methods should be used to back up a scientific statement. For example, for an immunoblot or protein electrophoresis gel, it is widely recognised that appropriate replication and comparative densitometry (with a good negative control) provide a simple way of making an otherwise singular result more robust. But for a live cellular process, such approaches are ill defined and many studies continue to be published where a hypothesis stands or falls backed up with by a singular striking image of a cell. In addition, it is obvious that in a biological system, no singular image could possibly encapsulate all eventualities. These issues are particularly relevant when the cell of interest is only a micron in length, as is the *Plasmodium* parasite, and the biological process is hard to capture, such as this parasite's entry into the human erythrocyte en route to causing malaria disease.

Here we have tried to address image bias and biological variability in the application of 3D immuno-fluorescence microscopy to merozoite invasion. Using recent advances in methods to capture and image the process of invasion of erythrocytes (Boyle et al., 2010b; Riglar et al., 2011) we have developed a workflow that creates a standardisation of imaging events permitting comparisons between samples to assess the distribution of various test proteins during invasion. Whilst at the resolution limits of deconvolution microscopy, our goal has been to provide a workflow that is possible to replicate using best practice fluorescence imaging on a conventional widefield microscope. The imaging for this requires no more than the ability to make a 3D z-stack and having access to good antibodies (Bordeaux et al., 2010). Using this approach, which we refer to as longitudinal intensity profiling, we assess whether the fluorescence signals associated with labelled proteins on the invading merozoite fit with the hypothesized function of those proteins.

Our approach makes several striking observations about the process of merozoite invasion and the application of fluorescence imaging. Most sobering is the recognition that multiple antibodies or epitopes (such as in polyclonal antiserum) are required in assessing localisation to avoid potential problems with singular epitopes being masked or poorly accessible under certain fixation conditions. This is clearly demonstrated with the distribution of the invasion protein AMA1. Whilst previous data has presented dual viewpoints about the presence (Alexander et al., 2005; Riglar et al., 2011) or absence (Giovannini et al., 2011) of AMA1 at the tight junction during apicomplexan parasite entry into host cells, here we show both scenarios can be explained, the latter the result of

masking of the antigen epitope targeted by the monoclonal antibody (Coley et al., 2007). This is likely to be the case for monoclonal antibodies used for imaging *Toxoplasma* AMA1 during tachyzoite invasion (Giovannini et al., 2011). Thus, our approach, we believe, clearly demonstrates that AMA1 does track the junction, however the longitudinal profile also shows that a large proportion of AMA1 is also carried in both within the apical complex (likely in unsecreted micronemes) or distributed variably on the invading parasites cell surface (Fig. 2; Fig. 7C).

Applying the workflow to imaging of motor components also reveals several insights. Foremost, actin concentrates and aldolase is present at or immediately behind the junction as the parasite enters (Fig. 3, 7C). Whilst current data that aldolase plays no force transduction role in the mechanics of parasite motility and invasion is now gaining acceptance (Shen and Sibley, 2014), it is entirely feasible that aldolase may nonetheless localise with the junction as the parasite invades. That is, energy production may be concentrated around the gliding motor during invasion, a concept that is consistent with, albeit contested (Starnes et al., 2009), evidence for relocalization of the glycolytic enzymes at this time (Pomel et al., 2008).

Whilst the localisation of actin and aldolase might fit with an evolving model of gliding motor organisation, our data on MTRAP leaves current understanding much more unresolved. The TRAP like proteins are envisaged to play an unbroken linkage between the intracellular actomyosin motor and the extracellular milieu (Baum et al., 2008). The absence of the adhesive TSR domain of MTRAP at the junction (Fig. 5) and accumulated evidence that it is pre-processed from the cytoplasmic domain well before invasion, likely prior to egress of merozoites from the infected erythrocyte (Figs 6, 7), question whether it can form an unbroken linkage with the internal gliding motor as originally envisaged (Baum et al., 2006b; Fig. 7C). Indeed, our own efforts at reciprocally immuno-precipitating the MTRAP head (TSR) and cytoplasmic tail were unsuccessful (data not shown) suggesting that post-processing the two parts of MTRAP may not even stay together. Recent evidence suggests that the shedding of the extracellular domain of liver stage TRAP is essential for both gliding motility and host infectivity (Ejigiri et al., 2012). Thus, what may be emerging is a sense that it is the processing and release of adhesive domains that either provides necessary signals to the parasite for motility/invasion or that may even provide a substrate for other adhesive ligands to bind. Further exploration of the function of adhesive domains in providing the conduit for motor traction will be important in resolving TRAP-like protein function (Hegge et al., 2010; Hellmann et al., 2013; Munter et al., 2009).

Thus we now believe it is entirely plausible that MTRAP plays no direct role in mediating invasion of the erythrocyte directly but may instead function in a signalling role either with the TSR binding to the erythrocyte surface (Bartholdson et al., 2012) on rupture priming the erythrocyte at invasion or some other binding event that does not require linkage to the junction or motor machinery. Our previous attempts to knockout MTRAP failed by conventional double cross-over recombination (Baum et al., 2006b). Additional attempts to knock down MTRAP levels using various conditional

knock-out systems, including both FKBP (Armstrong and Goldberg, 2007) and DHFR based destabilisation domains (Muralidharan et al., 2011) were unsuccessful (Fig. S3B-E). In each case, while integration of the respective domains occurred in almost all parasites within 2 integration cycles, no evidence for regulation of protein levels was seen. With recent advances in conditional genetic systems (Collins et al., 2013a; Yap et al., 2014) it may yet be possible to make a conditional knockout to explore the function of MTRAP directly and test whether its role relates to the mechanics of invasion or some other signalling event. Future work in this area is clearly of interest.

In summary, we present a coherent workflow for assessing the localisation of proteins during the transient process of *Plasmodium* merozoite invasion of the human erythrocyte. This approach, longitudinal intensity profiling, may be applicable to multiple cellular systems beyond parasite invasion. Our data highlight the importance of antibody selection, and multiple epitope targeting in generating unbiased fluorescence imaging data to test hypotheses. Absence of signal can still be explained by alternative hypotheses (such as epitope masking) in which case our data also stress the need for non-imaging methodologies to back up hypotheses of function, where protein localisation is unclear.

## MATERIALS AND METHODS

### *Parasite tissue culture, merozoite isolation*

*P. falciparum* D10-PfM3' asexual stage parasites (O'Donnell et al., 2001) were maintained using standard culture conditions in human O+ erythrocytes (Australian Red Cross Blood Bank, South Melbourne, Australia). Culture medium was RPMI-HEPES with 0.18% NaHCO<sub>3</sub> and 0.5% AlbumaxII (LifeTechnologies, Carlsbad, CA, USA) or 10% pooled human serum from unexposed donors (Australian Red Cross Blood Bank, South Melbourne, Australia). Parasites were synchronised using a combination of sorbitol (Sigma-Aldrich, St Louis, MO, USA) and heparin (Pfizer, New York, NY, USA) synchronisation methods (Boyle et al., 2010a; Lambros and Vanderberg, 1979).

Purified invasive merozoites were isolated and fixed during invasion as previously described (Riglar and Baum, 2013). Briefly, tightly synchronised late stage schizonts (>40 h) were isolated from >90 mL culture by magnet purification (MACS Miltenyi Biotech, Bergisch Gladbach, Germany) and treated with 10 µM E64 (Sigma-Aldrich, St Louis, MO, USA) for 6-8 h in >30 mL culture medium before being pelleted by centrifugation (1900 g, 5 min), resuspended in a small amount of serum-free media (typically >0.75 mL), filtered through a 1.2 µm, 32 mm syringe filter (Sartorius Stedim Biotech, Aubagne, France) and mixed immediately with fresh human erythrocytes (typically <15 µL of packed erythrocytes washed and resuspended at 50% in serum free culture medium) at 37°C with shaking. After 2 minutes, invading merozoites were fixed with 4% paraformaldehyde (ProSciTech, Thuringowa Central, QLD, Australia)/ 0.0075% glutaraldehyde (ProSciTech, Thuringowa Central, QLD, Australia) in PBS for 30 min at room temperature, followed by permeabilisation with 0.1% Triton-X 100 (Bio-Rad Laboratories, Hercules, CA, USA) for 10 min and blocking overnight or longer at 4°C with filtered 3% Bovine Serum Albumin (Sigma-Aldrich, St Louis, MO, USA) in PBS (blocking solution).

For schizont stage imaging, thin smears were taken directly from culture and air dried before being fixed in 100% methanol at -20°C for 30 seconds. After drying, slides were blocked for >30 min at RT with blocking solution.

For cleavage analysis synchronised parasites were treated with a combination of antipain and leupeptin (10 µg/mL of each; Sigma-Aldrich, St Louis, MO, USA), E-64 as described above, or pyrrole 4-[2-(4-fluorophenyl)-5-(1-methylpiperid ine-4-yl)-1H-pyrrol-3-yl] pyridine (Compound 1, SYNthesis Med Chem (Parkville, VIC, Australia); 2.5 µM) (Collins et al., 2013b).

### *Immunofluorescence detection of proteins*

Blocked invading parasites and schizont smears were incubated, in solution or on slide respectively, with primary antibodies diluted in blocking solution for 1 hour at room temperature. The following dilutions were used: mouse anti-RON4 (Richard et al., 2010), 1:500; rabbit anti-RON4 (Richard et al., 2010) 1:250; mouse anti-AMA1 1F9 (Coley et al., 2001) 1: 200; rabbit anti-

AMA1 R190 (Healer et al., 2002), 1: 200; rabbit anti-MTRAP TSR (Baum et al., 2006b) 1:50-1:100; rabbit anti-MTRAP MID (this study) 1:25; rabbit anti-MTRAP TAIL (this study) 1:250-1:500; rabbit anti-actin (Angrisano et al., 2012) 1:200; rabbit anti-aldolase (Baum et al., 2006b) 1:200; rabbit anti-GAP45 (Baum et al., 2006b) 1:200. Following primary incubation, samples were washed twice with PBS, incubated for 1 hour at room temperature with Alexa 488 or Alexa 594 conjugated secondary antibodies raised against the appropriate species diluted 1:500 in blocking solution (LifeTechnologies, Carlsbad, CA, USA), then washed three times with PBS. Invading merozoite samples were settled for 30 min at room temperature onto high-performance #1.5 grade coverslips (Carl Zeiss AG, Oberkochen, Germany) pre-flamed and coated with a 1% polyethyleneimine solution (Sigma-Aldrich, St Louis, MO, USA). Coverslips were mounted in VectaShield® (Vector Laboratories, Cambridgeshire, UK) with 0.1ng/μL 4',6-diamidino-2-phenylindole, DAPI (LifeTechnologies, Carlsbad, CA, USA). Results shown are representative of multiple experiments with antibodies tested empirically on each the day of use to control for batch-to-batch variation.

Imaging was performed on a DeltaVision Elite widefield microscope (Applied Precision), using a 100x/1.4NA Super-Plan APO oil-immersion objective (Olympus), InsightSSI solid-state illumination, and a CoolSnap HQ2 CCD camera (Photometrics). Filter sets used were DAPI (Ex: 390/18nm | Em:435/48nm), FITC (Ex: 475/28 | Em:525/48nm) and AlexaFluor594 (Ex: 575/25 | Em:625/45nm). Image stacks were captured well above and below the parasite with a z step of 150 nm and deconvolution undertaken in the DeltaVision SoftWoRx™ software package.

Image processing was routinely performed using ImageJ. A custom ImageJ macro, the Figure Wizard, was used extensively in creation of final figure panels used throughout this study. The Figure Wizard is available for download at [https://github.com/DrLachie/Figure\\_Wizard](https://github.com/DrLachie/Figure_Wizard)

#### *Immunoblot detection of proteins*

For immunoblot analysis tightly synchronised parasites were harvested by centrifugation at the appropriate time, released from erythrocytes in 1.5 volumes of 0.15% saponin + cOmplete protease inhibitor (Roche Applied Biosciences, Penzberg, Germany) for 10 min on ice, washed with ice cold PBS and solubilised in 2x SDS loading buffer. Proteins were separated on NuPAGE Novex 4-12% Bis-Tris gels with MES Buffer (LifeTechnologies, Carlsbad, CA, USA) and transferred to 0.2 μm PVDF membrane using the iBlot system ((LifeTechnologies, Carlsbad, CA, USA). Membranes were blocked in 5% (w/v) skim milk, 0.1% Tween-20 (Sigma-Aldrich, St Louis, MO, USA), PBS for 1 hr at room temperature then incubated for 1 hr with primary antisera diluted as follows in 1% (w/v) skim milk, 0.1% Tween-20, PBS: affinity purified rabbit anti-MTRAP tsr (rMtsr) 1:500 (Baum et al., 2006b); rabbit anti-MTRAPmid monoclonal (rMmid) 1:25 (this study); rabbit anti-MTRAP tail (rMtail) 1:1000 (this study); mouse anti-GFP monoclonal 1:1000 (clones 7.1/13.1, Roche Applied Biosciences, Penzberg, Germany); anti-MSP1 (Cooper et al., 1992) 1:1000. After washing, signal was detected with appropriate IgG horseradish peroxidase (HRP)

conjugates (Merck Millipore, Billerica, MA, USA), followed by further washes and chemiluminescence-detection (ECL, Amersham Biosciences, Little Chalfont, UK).

#### *Image acquisition and processing work flow for analysing multiple invasion events*

Invading free merozoites, were prepared for indirect immunofluorescence assay and imaged as described above. In each case the tight junction-associated protein RON4 (Richard et al., 2010) was included as one of two primary antibodies. Parasites were selected for imaging using three criteria: the presence of a clear ring of labelling with RON4 indicating a parasite close to the midpoint of invasion; invasion occurring approximately planar with the microscope's x-y plane; and the absence of confounding merozoites in the vicinity. The labelling of non-RON4 comparison antibodies was not taken into account. To analyse the distribution of antibody labelling along the length of a merozoite, images were rotationally aligned in the x-y direction (Fig. 1B i) and pixel intensity profiles were generated (Fig. 1B ii) in Metamorph Image Analysis software (Molecular Devices, Sunnyvale, CA, USA). To do so, values were recorded from a max intensity line profile with a line width of 45 that was taken for 50 pixels along the long axis in each direction from the brightest intensity point in the RON4 channel. This analysis was repeated for all z-positions, a process that adjusts for deviation from an x-y planar invasion vector (i.e. where invasion was tilted in the z-axis). Slices in which the profile spuriously centred to a point outside of the bounds, as defined from the DIC image, of the merozoite (e.g. due to background fluorescence) were discarded automatically. The resulting values were then summed for the whole z-stack and normalised to the maximum value across each parasite, resulting in a single average linear representation for the 3D longitudinal labelling distribution across each merozoite (Fig. 1B iii). Once generated, images were then assembled in a mock-temporal fashion i.e. assigning parasites to being *early* through *late* in the process of invasion as determined by the position of the junction relative to apex or base of the merozoite. This mock-temporal distribution was displayed using a heat map to present all available data for a given antibody collectively. Metamorph journals used for longitudinal intensity profiling are available at [https://github.com/DrLachie/Longitudinal\\_Intensity\\_Profiler](https://github.com/DrLachie/Longitudinal_Intensity_Profiler).

#### *MTRAP antiserum*

A synthetic peptide encompassing the C terminal residues of the MTRAP protein, N-CYFLRKEKTEKVVQEETKEENFEVMFNDDALKGKDNKAMDEEEFWALE-C, was used to generate rabbit polyclonal serum (GenScript Piscataway, NJ, USA). A recombinant protein encompassing Valine (residue 95) to Glutamic Acid (residue 299) was generated by PCR amplification from *P. falciparum* genomic DNA, cloned by restriction enzyme digestion into a BamHI-XhoI digested expression vector (pGEX-4T-1, GE Healthcare Biosciences AB, Uppsala Sweden) and expressed as a recombinant protein in *Escherichia coli* (strain BL21). The protein was purified over glutathione agarose (Sigma-Aldrich, St Louis, MO, USA) using conventional methods (Baum et al., 2006b). The purified protein was used to immunise rabbits and generate

both polyclonal and a monoclonal antibody (clone 3A3, Walter and Eliza Hall Monoclonal Facility, Bundoora, VIC, Australia).

#### *Vector construction and generation of destabilisation domain mutations and their analysis*

All PCR primers and vector maps are available on request. A derivative of the FKBP destabilization domain, DDtm, (Chu et al., 2008) and a DHFR degradation domain (DDD) (Iwamoto et al., 2010), both of which have previously been used to successfully regulate proteins in *P. falciparum* (Dvorin et al., 2010; Muralidharan et al., 2011) were generated as C-terminal fusions of MTRAP. Fragments of either DDD (derived by PCR from the published vector (Muralidharan et al., 2011)) or DDtm (ordered as a synthetic DNA construct (Geneart, LifeTechnologies, Carlsbad, CA, USA)) were inserted into the vector pD3HA (Riglar et al., 2011) into sites NheI and NcoI (replacing the triple HA tag). For the DDD vector, the DHFR selection cassette was replaced with one encoding blasticidin deaminase (Bsd), conferring resistance to blasticidin-S (Bs). Upstream of the inserted tag, an 813 bp 3' flank ending at (but excluding) MTRAP's stop codon was PCR amplified and cloned in front of each domain to include a triple alanine linker in frame with either the DDtm or DDD sequence generating plasmids pMTRAP-DDtm and pMTRAP-DDD. D10 and 3D7ΔRh3 parasites (the latter used for its integrated DHFR resistance (Baum et al., 2005), necessary to confer resistance to the trimethoprim (TMP) ligand) were transfected with respective DDtm and DDD plasmids using standard methods (Riglar et al., 2011), and selected with WR99210 or bsd respectively and grown in the presence of either 2 μM shield-1 (for DDtm) or 10 μM TMP (for DDD). Integration of 3' tags were assessed after two cycles, at which point the regulation of MTRAP was tested. To test MTRAP regulation parasites were tightly synchronised washed at ring stage and grown in the presence or absence of respective ligand. These conditions were maintained for two or three cycles for DDtm and DDD experiments respectively, concurrently measuring parasitemia and taking protein samples for immuno-blot analysis. 3D7ΔRh3 MTRAP-DDD parasites were also maintained over long-term standard culture in the absence of TMP to test regulation.

## ACKNOWLEDGEMENTS

The authors thank Rachel Gillespie for experimental support and helpful discussion and Robin Anders for allowing access to monoclonal antibodies. Use of human red blood cells for parasite work was approved by the Walter and Eliza Hall Human Research Ethics Committee (ethics number 86/17) and an Australian Red Cross Blood Service Agreement (11-09VIC-01). Experimental data presented here was made possible through Victorian State Government Operational Infrastructure Support and Australian Government NHMRC IRIISS. The research was directly supported by a National Health and Medical Research Council of Australia (NHMRC) Project Grant (APP1047085, JB), Program Grant (637406, AFC) and a Human Frontier Science Program (HFSP) Young Investigator Program Grant (RGY0071/2011, JB). DTR was supported during this work by a Pratt Foundation postgraduate scholarship through the University of Melbourne. AFC is an International Scholar of the Howard Hughes Medical Institute. JB was supported through a Future Fellowship (FT100100112) from the ARC and is currently supported by the Wellcome Trust, through a New Investigator Award (100993/Z/13/Z). **The authors declare no conflict of interest.**

**Author contributions:** DTR, LW, KR, and JB worked closely together to design, perform and interpret experiments; AFC provided invaluable access to antibody resources and intellectual support for the project. DTR and JB wrote the paper.

## REFERENCES

- Aikawa, M., Miller, L. H., Johnson, J. and Rabbege, J.** (1978). Erythrocyte entry by malarial parasites. A moving junction between erythrocyte and parasite. *J Cell Biol* **77**, 72-82.
- Alexander, D. L., Mital, J., Ward, G. E., Bradley, P. and Boothroyd, J. C.** (2005). Identification of the Moving Junction Complex of *Toxoplasma gondii*: A Collaboration between Distinct Secretory Organelles. *PLoS Pathog* **1**, e17.
- Andenmatten, N., Egarter, S., Jackson, A. J., Jullien, N., Herman, J. P. and Meissner, M.** (2013). Conditional genome engineering in *Toxoplasma gondii* uncovers alternative invasion mechanisms. *Nat Methods* **10**, 125-7.
- Angrisano, F., Riglar, D. T., Sturm, A., Volz, J. C., Delves, M. J., Zuccala, E. S., Turnbull, L., Dekiwadia, C., Olshina, M. A., Marapana, D. S. et al.** (2012). Spatial localisation of actin filaments across developmental stages of the malaria parasite. *PLoS One* **7**, e32188.
- Armstrong, C. M. and Goldberg, D. E.** (2007). An FKBP destabilization domain modulates protein levels in *Plasmodium falciparum*. *Nat Methods* **4**, 1007-9.
- Baker, R. P., Wijetilaka, R. and Urban, S.** (2006). Two *Plasmodium* rhomboid proteases preferentially cleave different adhesins implicated in all invasive stages of malaria. *PLoS Pathog* **2**, e113.
- Bannister, L. H., Butcher, G. A., Dennis, E. D. and Mitchell, G. H.** (1975). Structure and invasive behaviour of *Plasmodium knowlesi* merozoites in vitro. *Parasitology* **71**, 483-91.
- Bannister, L. H. and Mitchell, G. H.** (2009). The malaria merozoite, forty years on. *Parasitology* **136**, 1435-44.
- Bargieri, D. Y., Andenmatten, N., Lagal, V., Thiberge, S., Whitelaw, J. A., Tardieux, I., Meissner, M. and Menard, R.** (2013). Apical membrane antigen 1 mediates apicomplexan parasite attachment but is dispensable for host cell invasion. *Nat Commun* **4**, 2552.
- Bartholdson, S. J., Bustamante, L. Y., Crosnier, C., Johnson, S., Lea, S., Rayner, J. C. and Wright, G. J.** (2012). Semaphorin-7A Is an Erythrocyte Receptor for *P. falciparum* Merozoite-Specific TRAP Homolog, MTRAP. *PLoS Pathog* **8**, e1003031.
- Baum, J., Gilberger, T.-W., Frischknecht, F. and Meissner, M.** (2008). Host-cell invasion by malaria parasites: insights from *Plasmodium* and *Toxoplasma*. *Trends Parasitol* **24**, 557-63.
- Baum, J., Maier, A. G., Good, R. T., Simpson, K. M. and Cowman, A. F.** (2005). Invasion by *P. falciparum* Merozoites Suggests a Hierarchy of Molecular Interactions. *PLoS Pathog* **1**, e37.
- Baum, J., Papenfuss, A. T., Baum, B., Speed, T. P. and Cowman, A. F.** (2006a). Regulation of apicomplexan actin-based motility. *Nat Rev Microbiol* **4**, 621-8.
- Baum, J., Richard, D., Healer, J., Rug, M., Krnajska, Z., Gilberger, T.-W., Green, J. L., Holder, A. A. and Cowman, A. F.** (2006b). A conserved molecular motor drives cell invasion and gliding motility across malaria life cycle stages and other apicomplexan parasites. *J Biol Chem* **281**, 5197-208.
- Bichet, M., Joly, C., Henni, A., Guilbert, T., Xemard, M., Tafani, V., Lagal, V., Charras, G. and Tardieux, I.** (2014). The toxoplasma-host cell junction is anchored to the cell cortex to sustain parasite invasive force. *BMC Biol* **12**, 773.
- Bordeaux, J., Welsh, A., Agarwal, S., Killiam, E., Baquero, M., Hanna, J., Anagnostou, V. and Rimm, D.** (2010). Antibody validation. *Biotechniques* **48**, 197-209.
- Boyle, M. J., Langer, C., Chan, J. A., Hodder, A. N., Coppel, R. L., Anders, R. F. and Beeson, J. G.** (2014). Sequential processing of merozoite surface proteins during and after erythrocyte invasion by *Plasmodium falciparum*. *Infect Immun* **82**, 924-36.
- Boyle, M. J., Richards, J. S., Gilson, P. R., Chai, W. and Beeson, J. G.** (2010a). Interactions with heparin-like molecules during erythrocyte invasion by *Plasmodium falciparum* merozoites. *Blood* **115**, 4559-68.
- Boyle, M. J., Wilson, D. W., Richards, J. S., Riglar, D. T., Tetteh, K. K., Conway, D. J., Ralph, S. A., Baum, J. and Beeson, J. G.** (2010b). Isolation of viable *Plasmodium falciparum* merozoites

- to define erythrocyte invasion events and advance vaccine and drug development. *Proc Natl Acad Sci USA* **107**, 14378-83.
- Chu, B. W., Banaszynski, L. A., Chen, L. C. and Wandless, T. J.** (2008). Recent progress with FKBP-derived destabilizing domains. *Bioorg Med Chem Lett* **18**, 5941-4.
- Coley, A. M., Campanale, N. V., Casey, J. L., Hodder, A. N., Crewther, P. E., Anders, R. F., Tilley, L. M. and Foley, M.** (2001). Rapid and precise epitope mapping of monoclonal antibodies against *Plasmodium falciparum* AMA1 by combined phage display of fragments and random peptides. *Protein Eng* **14**, 691-8.
- Coley, A. M., Gupta, A., Murphy, V. J., Bai, T., Kim, H., Foley, M., Anders, R. F. and Batchelor, A. H.** (2007). Structure of the malaria antigen AMA1 in complex with a growth-inhibitory antibody. *PLoS Pathog* **3**, 1308-19.
- Collins, C. R., Das, S., Wong, E. H., Andenmatten, N., Stallmach, R., Hackett, F., Herman, J. P., Muller, S., Meissner, M. and Blackman, M. J.** (2013a). Robust inducible Cre recombinase activity in the human malaria parasite *Plasmodium falciparum* enables efficient gene deletion within a single asexual erythrocytic growth cycle. *Mol Microbiol* **88**, 687-701.
- Collins, C. R., Hackett, F., Strath, M., Penzo, M., Withers-Martinez, C., Baker, D. A. and Blackman, M. J.** (2013b). Malaria parasite cGMP-dependent protein kinase regulates blood stage merozoite secretory organelle discharge and egress. *PLoS Pathog* **9**, e1003344.
- Cooper, J. A., Cooper, L. T. and Saul, A. J.** (1992). Mapping of the region predominantly recognized by antibodies to the *Plasmodium falciparum* merozoite surface antigen MSA 1. *Mol Biochem Parasitol* **51**, 301-12.
- Cowman, A. F., Berry, D. and Baum, J.** (2012). The cellular and molecular basis for malaria parasite invasion of the human red blood cell. *J Cell Biol* **198**, 961-71.
- Drewry, L. L. and Sibley, L. D.** (2015). Toxoplasma Actin Is Required for Efficient Host Cell Invasion. *MBio* **6**.
- Dvorak, J. A., Miller, L. H., Whitehouse, W. C. and Shiroishi, T.** (1975). Invasion of erythrocytes by malaria merozoites. *Science* **187**, 748-50.
- Dvorin, J. D., Martyn, D. C., Patel, S. D., Grimley, J. S., Collins, C. R., Hopp, C. S., Bright, A. T., Westenberger, S., Winzeler, E., Blackman, M. J. et al.** (2010). A plant-like kinase in *Plasmodium falciparum* regulates parasite egress from erythrocytes. *Science* **328**, 910-2.
- Egarter, S., Andenmatten, N., Jackson, A. J., Whitelaw, J. A., Pall, G., Black, J. A., Ferguson, D. J., Tardieux, I., Mogilner, A. and Meissner, M.** (2014). The toxoplasma Acto-MyoA motor complex is important but not essential for gliding motility and host cell invasion. *PLoS One* **9**, e91819.
- Ejigiri, I., Ragheb, D. R., Pino, P., Coppi, A., Bennett, B. L., Soldati-Favre, D. and Sinnis, P.** (2012). Shedding of TRAP by a rhomboid protease from the malaria sporozoite surface is essential for gliding motility and sporozoite infectivity. *PLoS Pathog* **8**, e1002725.
- Giovannini, D., Späth, S., Lacroix, C., Perazzi, A., Bargieri, D., Lagal, V., Lebugle, C., Combe, A., Thiberge, S., Baldacci, P. et al.** (2011). Independent Roles of Apical Membrane Antigen 1 and Rhoptry Neck Proteins during Host Cell Invasion by Apicomplexa. *Cell Host Microbe* **10**, 591-602.
- Hanssen, E., Dekiwadia, C., Riglar, D. T., Rug, M., Lemgruber, L., Cowman, A. F., Cyrklaff, M., Kudryashev, M., Frischknecht, F., Baum, J. et al.** (2013). Electron tomography of *Plasmodium falciparum* merozoites reveals core cellular events that underpin erythrocyte invasion. *Cell Microbiol* **15**, 1457-1472.
- Healer, J., Crawford, S., Ralph, S., McFadden, G. and Cowman, A. F.** (2002). Independent translocation of two micronemal proteins in developing *Plasmodium falciparum* merozoites. *Infect Immun* **70**, 5751-8.
- Hegge, S., Munter, S., Steinbuchel, M., Heiss, K., Engel, U., Matuschewski, K. and Frischknecht, F.** (2010). Multistep adhesion of *Plasmodium* sporozoites. *FASEB J* **24**, 2222-34.
- Hellmann, J. K., Perschmann, N., Spatz, J. P. and Frischknecht, F.** (2013). Tunable substrates unveil chemical complementation of a genetic cell migration defect. *Adv Healthc Mater* **2**, 1162-9.

- Iwamoto, N., Lu, R., Tanaka, N., Abe-Dohmae, S. and Yokoyama, S.** (2010). Calmodulin interacts with ATP binding cassette transporter A1 to protect from calpain-mediated degradation and upregulates high-density lipoprotein generation. *Arterioscler Thromb Vasc Biol* **30**, 1446-52.
- Lamarque, M., Besteiro, S., Papoin, J., Roques, M., Vulliez-Le Normand, B., Morlon-Guyot, J., Dubremetz, J. F., Fauquenoy, S., Tomavo, S., Faber, B. W. et al.** (2011). The RON2-AMA1 interaction is a critical step in moving junction-dependent invasion by apicomplexan parasites. *PLoS Pathog* **7**, e1001276.
- Lamarque, M. H., Roques, M., Kong-Hap, M., Tonkin, M. L., Rugarabamu, G., Marq, J. B., Penarete-Vargas, D. M., Boulanger, M. J., Soldati-Favre, D. and Lebrun, M.** (2014). Plasticity and redundancy among AMA-RON pairs ensure host cell entry of Toxoplasma parasites. *Nat Commun* **5**, 4098.
- Lambros, C. and Vanderberg, J. P.** (1979). Synchronization of Plasmodium falciparum erythrocytic stages in culture. *J Parasitol* **65**, 418-20.
- Lingelbach, K. and Joiner, K. A.** (1998). The parasitophorous vacuole membrane surrounding Plasmodium and Toxoplasma: an unusual compartment in infected cells. *J Cell Sci* **111 ( Pt 11)**, 1467-75.
- Munter, S., Sabass, B., Selhuber-Unkel, C., Kudryashev, M., Hegge, S., Engel, U., Spatz, J. P., Matuschewski, K., Schwarz, U. S. and Frischknecht, F.** (2009). Plasmodium sporozoite motility is modulated by the turnover of discrete adhesion sites. *Cell Host Microbe* **6**, 551-62.
- Muralidharan, V., Oksman, A., Iwamoto, M., Wandless, T. J. and Goldberg, D. E.** (2011). Asparagine repeat function in a Plasmodium falciparum protein assessed via a regulatable fluorescent affinity tag. *Proc Natl Acad Sci U S A* **108**, 4411-6.
- North, A. J.** (2006). Seeing is believing? A beginners' guide to practical pitfalls in image acquisition. *J Cell Biol* **172**, 9-18.
- O'Donnell, R. A. and Blackman, M. J.** (2005). The role of malaria merozoite proteases in red blood cell invasion. *Curr Opin Microbiol* **8**, 422-7.
- O'Donnell, R. A., de Koning-Ward, T. F., Burt, R. A., Bockarie, M., Reeder, J. C., Cowman, A. F. and Crabb, B. S.** (2001). Antibodies against merozoite surface protein (MSP)-1(19) are a major component of the invasion-inhibitory response in individuals immune to malaria. *J Exp Med* **193**, 1403-12.
- O'Donnell, R. A., Hackett, F., Howell, S. A., Treeck, M., Struck, N., Krnajski, Z., Withers-Martinez, C., Gilberger, T. W. and Blackman, M. J.** (2006). Intramembrane proteolysis mediates shedding of a key adhesin during erythrocyte invasion by the malaria parasite. *J Cell Biol* **174**, 1023-33.
- Pomel, S., Luk, F. C. and Beckers, C. J.** (2008). Host cell egress and invasion induce marked relocations of glycolytic enzymes in Toxoplasma gondii tachyzoites. *PLoS Pathog* **4**, e1000188.
- Richard, D., MacRaild, C. A., Riglar, D. T., Chan, J.-A., Foley, M., Baum, J., Ralph, S. A., Norton, R. S. and Cowman, A. F.** (2010). Interaction between Plasmodium falciparum apical membrane antigen 1 and the rhoptry neck protein complex defines a key step in the erythrocyte invasion process of malaria parasites. *J Biol Chem* **285**, 14815-22.
- Riglar, D. T. and Baum, J.** (2013). Static and dynamic imaging of erythrocyte invasion and early intra-erythrocytic development in Plasmodium falciparum. *Methods Mol Biol* **923**, 269-80.
- Riglar, D. T., Richard, D., Wilson, D. W., Boyle, M. J., Dekiwadia, C., Turnbull, L., Angrisano, F., Marapana, D. S., Rogers, K. L., Whitchurch, C. B. et al.** (2011). Super-Resolution Dissection of Coordinated Events during Malaria Parasite Invasion of the Human Erythrocyte. *Cell Host Microbe* **9**, 9-20.
- Riglar, D. T., Rogers, K. L., Hanssen, E., Turnbull, L., Bullen, H. E., Charnaud, S. C., Przyborski, J., Gilson, P. R., Whitchurch, C. B., Crabb, B. S. et al.** (2013). Spatial association with PTEX complexes defines regions for effector export into Plasmodium falciparum-infected erythrocytes. *Nat Commun* **4**, 1415.
- Salmon, B. L., Oksman, A. and Goldberg, D. E.** (2001). Malaria parasite exit from the host erythrocyte: a two-step process requiring extraerythrocytic proteolysis. *Proc Natl Acad Sci U S A* **98**, 271-6.

- Sauer, M.** (2013). Localization microscopy coming of age: from concepts to biological impact. *J Cell Sci* **126**, 3505-13.
- Shen, B. and Sibley, L. D.** (2014). Toxoplasma aldolase is required for metabolism but dispensable for host-cell invasion. *Proc Natl Acad Sci U S A* **111**, 3567-72.
- Srinivasan, P., Beatty, W. L., Diouf, A., Herrera, R., Ambroggio, X., Moch, J. K., Tyler, J. S., Narum, D. L., Pierce, S. K., Boothroyd, J. C. et al.** (2011). Binding of Plasmodium merozoite proteins RON2 and AMA1 triggers commitment to invasion. *Proc Natl Acad Sci U S A* **108**, 13275-80.
- Starnes, G. L., Coincon, M., Sygusch, J. and Sibley, L. D.** (2009). Aldolase is essential for energy production and bridging adhesin-actin cytoskeletal interactions during parasite invasion of host cells. *Cell Host Microbe* **5**, 353-64.
- Tonkin, M. L., Roques, M., Lamarque, M. H., Pugniere, M., Douguet, D., Crawford, J., Lebrun, M. and Boulanger, M. J.** (2011). Host cell invasion by apicomplexan parasites: insights from the co-structure of AMA1 with a RON2 peptide. *Science* **333**, 463-7.
- Tyler, J. S. and Boothroyd, J. C.** (2011). The C-terminus of Toxoplasma RON2 provides the crucial link between AMA1 and the host-associated invasion complex. *PLoS Pathog* **7**, e1001282.
- Tyler, J. S., Treeck, M. and Boothroyd, J. C.** (2011). Focus on the ringleader: the role of AMA1 in apicomplexan invasion and replication. *Trends Parasitol* **27**, 410-20.
- Waters, J. C. and Wittmann, T.** (2014). Concepts in quantitative fluorescence microscopy. *Methods Cell Biol* **123**, 1-18.
- Weiss, G. E., Gilson, P. R., Taechalertpaisarn, T., Tham, W. H., de Jong, N. W., Harvey, K. L., Fowkes, F. J., Barlow, P. N., Rayner, J. C., Wright, G. J. et al.** (2015). Revealing the sequence and resulting cellular morphology of receptor-ligand interactions during Plasmodium falciparum invasion of erythrocytes. *PLoS Pathog* **11**, e1004670.
- White, N. J., Pukrittayakamee, S., Hien, T. T., Faiz, M. A., Mokuolu, O. A. and Dondorp, A. M.** (2014). Malaria. *Lancet* **383**, 723-35.
- Wickham, M. E., Culvenor, J. G. and Cowman, A. F.** (2003). Selective inhibition of a two-step egress of malaria parasites from the host erythrocyte. *J Biol Chem* **278**, 37658-63.
- Wong, W., Skau, C. T., Marapana, D. S., Hanssen, E., Taylor, N. L., Riglar, D. T., Zuccala, E. S., Angrisano, F., Lewis, H., Catimel, B. et al.** (2011). Minimal requirements for actin filament disassembly revealed by structural analysis of malaria parasite actin-depolymerizing factor 1. *Proc Natl Acad Sci U S A* **108**, 9869-74.
- Yap, A., Azevedo, M. F., Gilson, P. R., Weiss, G. E., O'Neill, M. T., Wilson, D. W., Crabb, B. S. and Cowman, A. F.** (2014). Conditional expression of apical membrane antigen 1 in Plasmodium falciparum shows it is required for erythrocyte invasion by merozoites. *Cell Microbiol* **16**, 642-56.
- Zhan, M., Crane, M. M., Entchev, E. V., Caballero, A., Fernandes de Abreu, D. A., Ch'ng, Q. and Lu, H.** (2015). Automated Processing of Imaging Data through Multi-tiered Classification of Biological Structures Illustrated Using Caenorhabditis elegans. *PLoS Comput Biol* **11**, e1004194.
- Zuccala, E. S. and Baum, J.** (2011). Cytoskeletal and membrane remodelling during malaria parasite invasion of the human erythrocyte. *Br J Haematol* **154**, 680-689.
- Zuccala, E. S., Gout, A. M., Dekiwadia, C., Marapana, D. S., Angrisano, F., Turnbull, L., Riglar, D. T., Rogers, K. L., Whitchurch, C. B., Ralph, S. A. et al.** (2012). Subcompartmentalisation of proteins in the rhoptries correlates with ordered events of erythrocyte invasion by the blood stage malaria parasite. *PLoS One* **7**, e46160.

# Figures

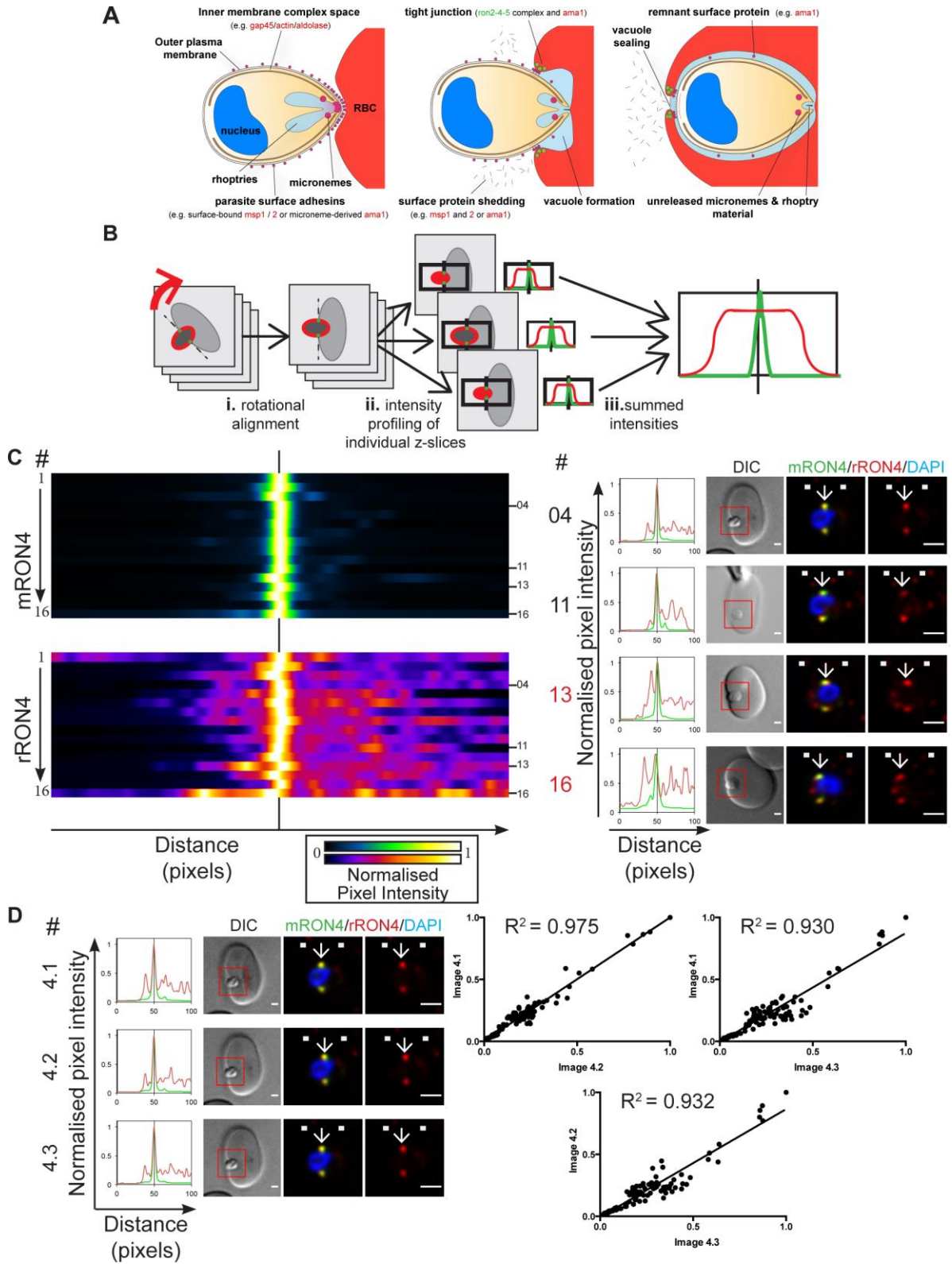


**Figure 1. A workflow for longitudinal intensity profiling of proteins during merozoite invasion.** **A)** Schematic of merozoite invasion showing stages of invasion, tight junction formation, micronemal and rhoptry release and surface protein shedding with some examples of key proteins involved. **B)** To analyse the localisation of proteins during invasion with respect to the tight junction in an unbiased manner, invading merozoites labelled for RON4 and another antibody of interest were chosen for imaging based on RON4 labelling and orientation and imaged by widefield fluorescence deconvolution microscopy. (i) Images were rotated so as to align invading left-to-right along the x-axis of the image and (ii) were then analysed using a max intensity plot profile along the long axis of the merozoite, centred to the brightest point in the RON4 labelled channel. (iii) Pixel intensity values were then summed to provide an average longitudinal distribution for each merozoite. **C)** Heatmaps (left), normalised intensity plots and single-slice images of four example merozoites which are referred to directly in the text (right) for the longitudinal intensity profiling of mRON4 (green) vs rRON4 (red) demonstrated the validity of this technique. See also Fig. S1A. **D)** Confirmation of workflow accuracy. Three independent replicate images of a single invading merozoite (left) were analysed for correlation by plotting corresponding values from the normalised longitudinal intensity profiles against one another (right). For all, scale bars = 1  $\mu\text{m}$ . Red boxes in DIC images indicate zoomed regions for middle and right panels. Arrows indicate the position of the RON4 labelled tight junction.

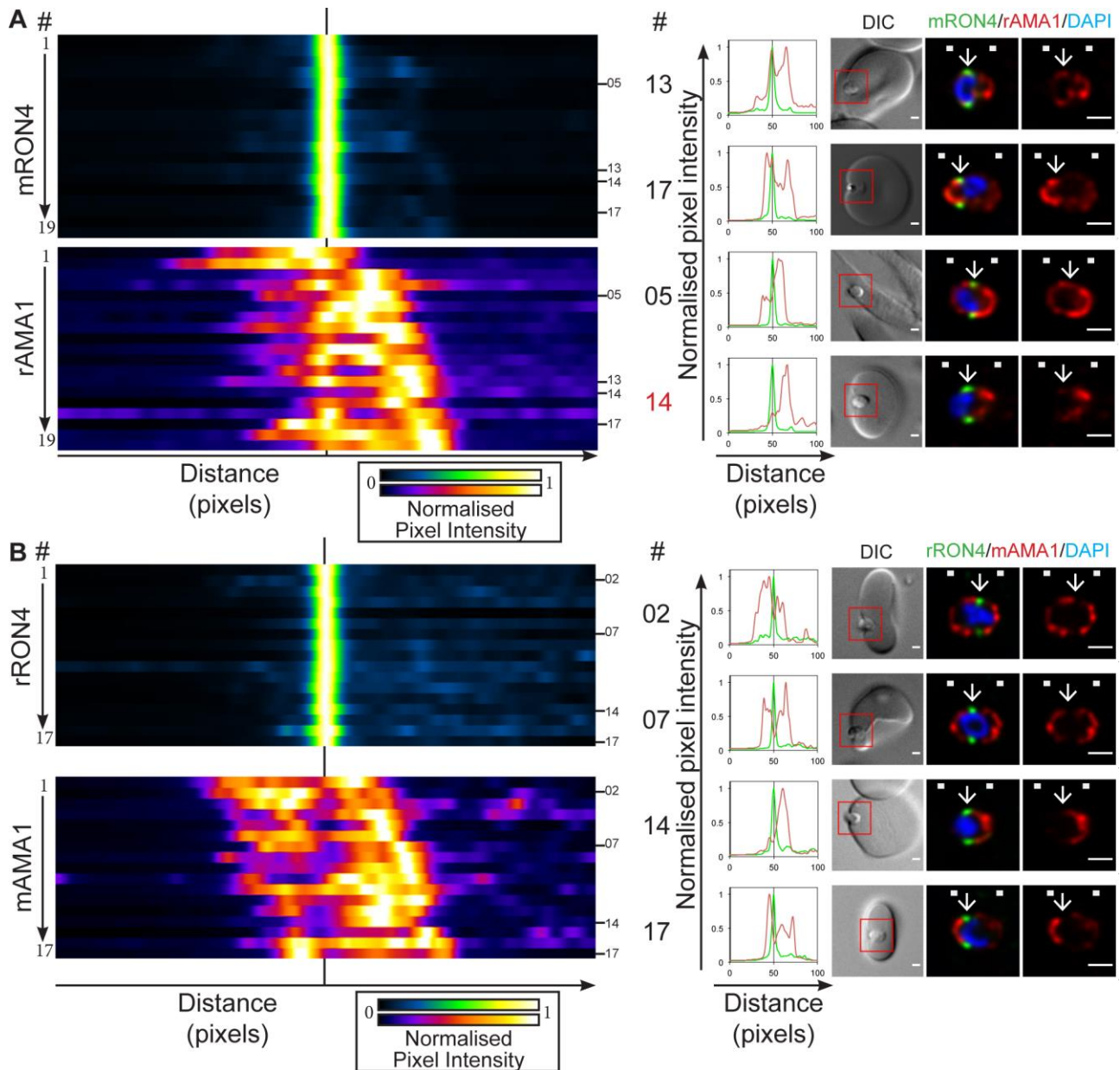


**Figure 2. Longitudinal intensity profiling demonstrates antibody specific variation in AMA1 localisation at the tight junction.** Heatmaps (left), normalised intensity plots and single-slice images of example merozoites (right) for the longitudinal intensity profiling of **A**) mRON4 (green) vs rAMA1 (red) or **B**) rRON4 (green) vs mAMA1 (red). Scale bars = 1  $\mu$ m. Red boxes in DIC images indicate zoomed regions for middle and right panels. Arrows indicate the position of the RON4 labelled tight junction. See also Fig. S1B-C.

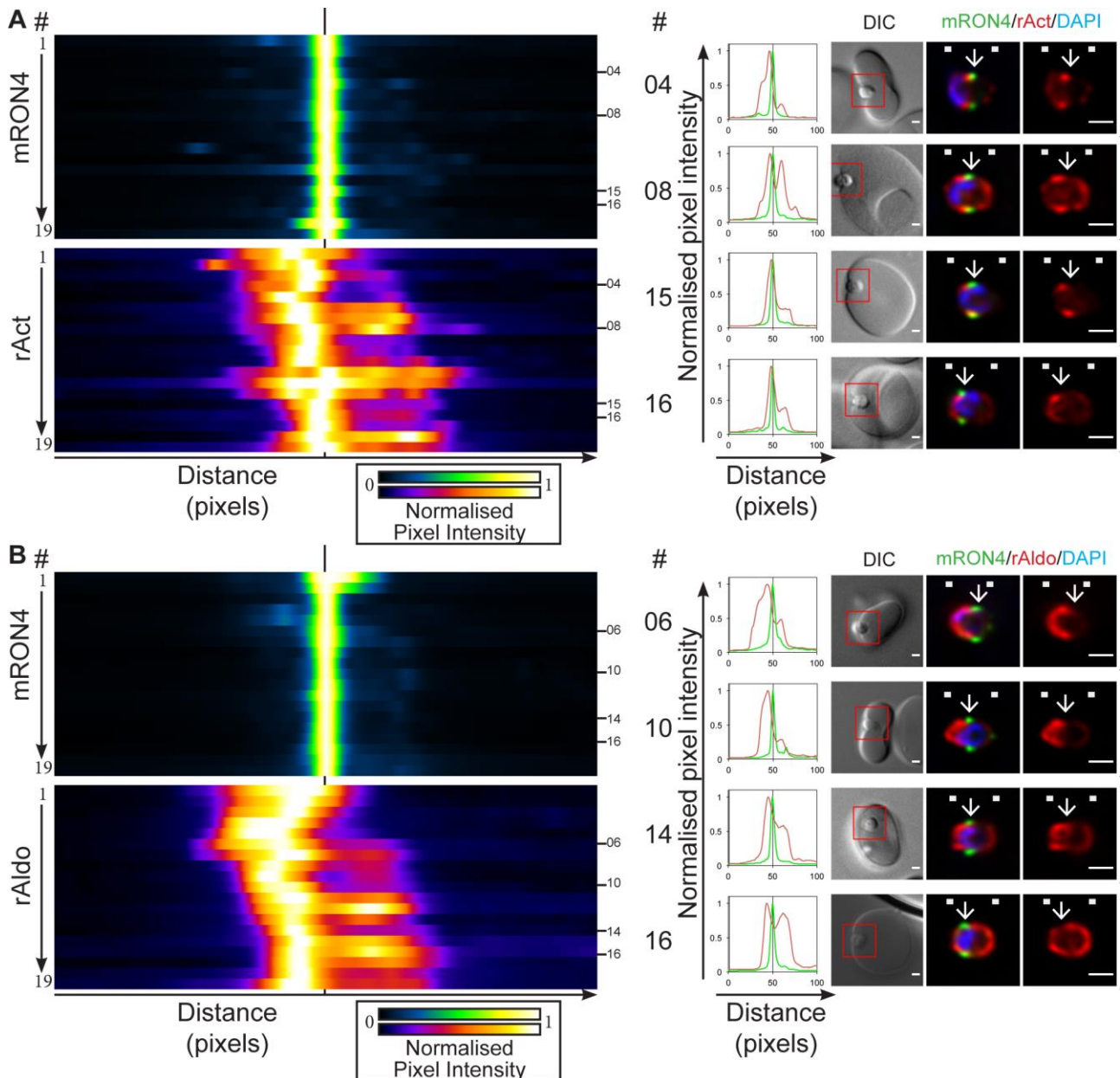


**Figure 3. Longitudinal intensity profiling localises actin and aldolase towards the rear of the invading merozoite's tight junction.** Heatmaps (left), normalised intensity plots and single-slice images of example merozoites (right) for the longitudinal intensity profiling of mRON4 (green) vs **A**) rActin (rAct) (red) or **B**) rAldolase (rAldo) (red). Scale bars = 1  $\mu$ m. Red boxes in DIC images indicate zoomed regions for middle and right panels. Arrows indicate the position of the RON4 labelled tight junction. See also Fig. S1D-E.

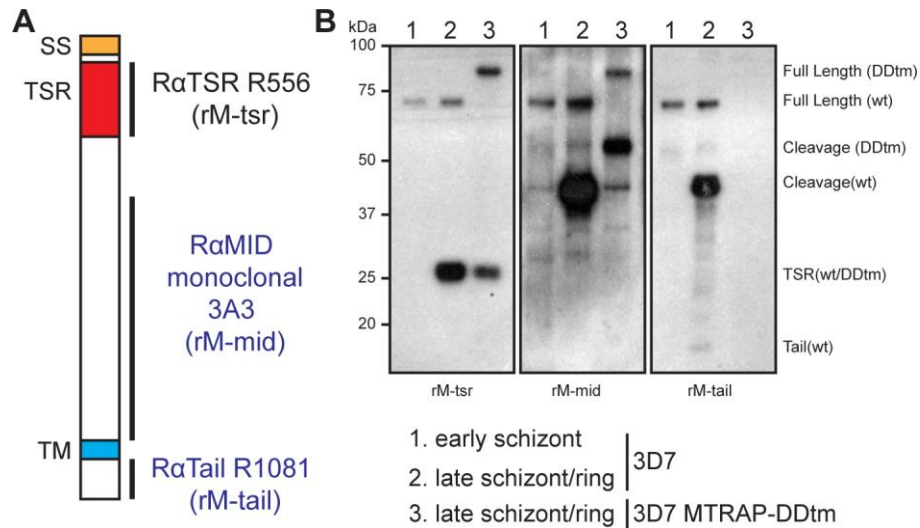


**Figure 4. MTRAP organisation and profile of domain-specific antibodies.** **A)** MTRAP consists of a signal sequence (SS, orange), two thrombospondin repeat domains (TSR, red), and a single transmembrane domain (TM, blue), with a short C-terminal cytoplasmic tail. In order to track MTRAP's various cleavage products we generated a rabbit monoclonal antibody (3A3) against the unstructured mid domain of MTRAP (rM-mid) and rabbit antiserum (R1081) against the short C-terminal tail of MTRAP (rM-tail). These antibodies complement the previously published MTRAP TSR (R556) antiserum (rM-tsr). **B)** Analysis of 3D7 schizont and mixed schizont/ring stage parasites along with schizont/ring stage parasites expressing a DD<sub>tm</sub> tagged version of MTRAP was used to test antibody recognition. Immuno-blot analysis labelled with rM-tsr antiserum identified full length MTRAP<sub>wt</sub> at ~75 kDa, full length MTRAP<sub>DDtm</sub> at ~90 kDa, and the cleaved MTRAP TSR domain at ~27 kDa in both late schizont/ring samples as expected. rM-mid antibodies also recognised the full length products, demonstrating its ability to specifically label MTRAP. Additionally, rM-mid recognised at least 1 product at ~44 kDa in 3D7 samples. A corresponding band running at ~55 kDa in MTRAP-DDtm tagged parasites confirms this is a cleavage product of MTRAP which maintains its C-terminal tail. In some samples a second cleavage product running at ~38 kDa was also seen (data not shown). rM-tail antiserum recognised the same full length and cleavage products in 3D7 samples. Additionally, a faint band was consistently labelled running at ~15 kDa in samples involving early ring stage parasites, but was absent in schizont stage parasites. We believe this corresponds to the MTRAP C-terminal tail stub following intramembrane cleavage. rM-tail antiserum was unable to label C-terminally tagged versions of MTRAP.

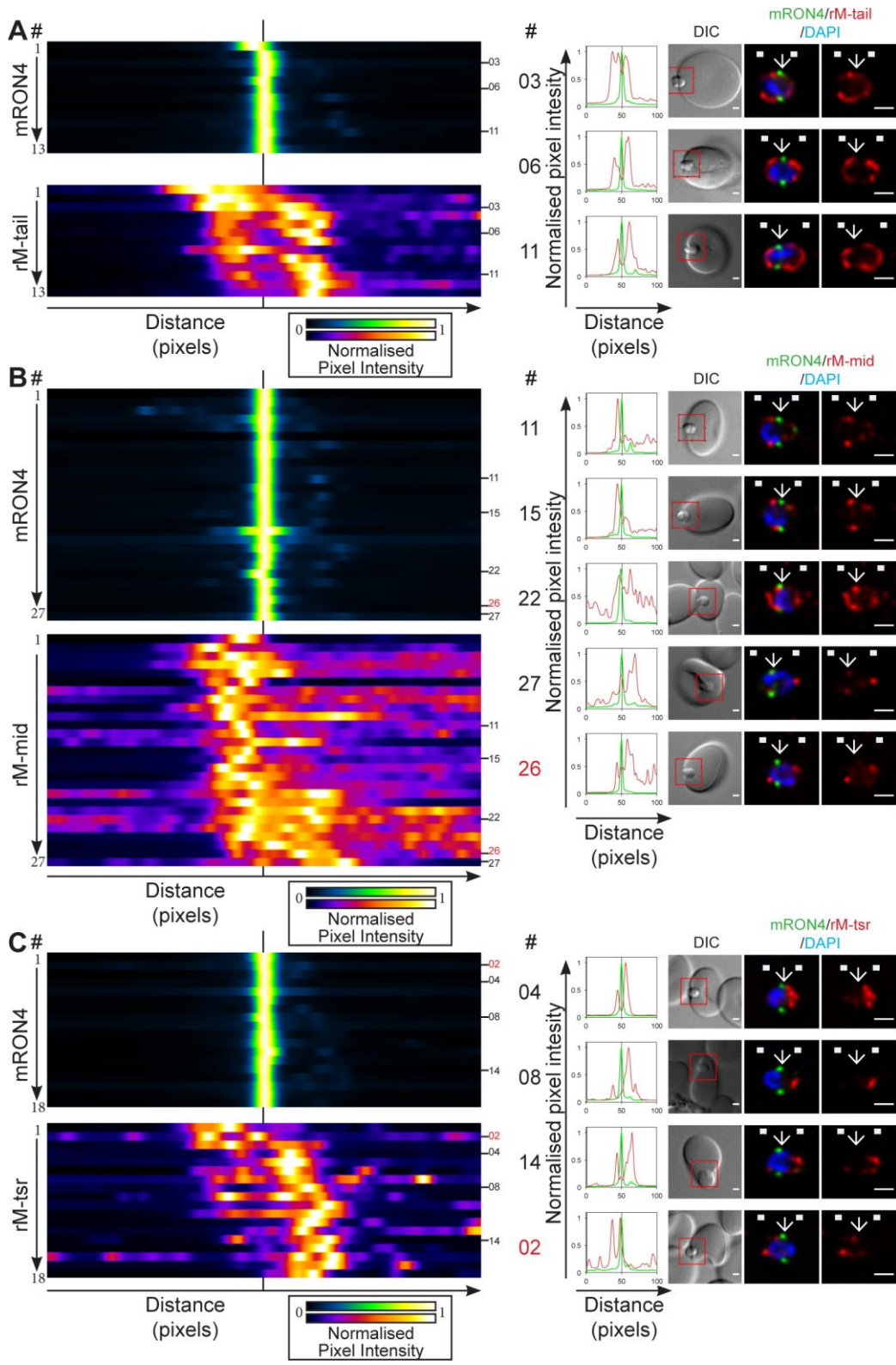


**Figure 5. Longitudinal intensity profiling identifies unexpected localisation profiles for MTRAP during merozoite invasion. A-C).** Heatmaps (left), normalised intensity plots and single-slice images of example merozoites (right) for the longitudinal intensity profiling of mRON4 (green) vs **A)** rMTRAP-tail (rM-tail) (red), **B)** rMTRAP mid (rM-mid) (red), or **C)** rMTRAP tsr (rM-tsr). Scale bars = 1  $\mu$ m. Red boxes in DIC images indicate zoomed regions for middle and right panels. Arrows indicate the position of the RON4 labelled tight junction. See also Fig. S2A-C.

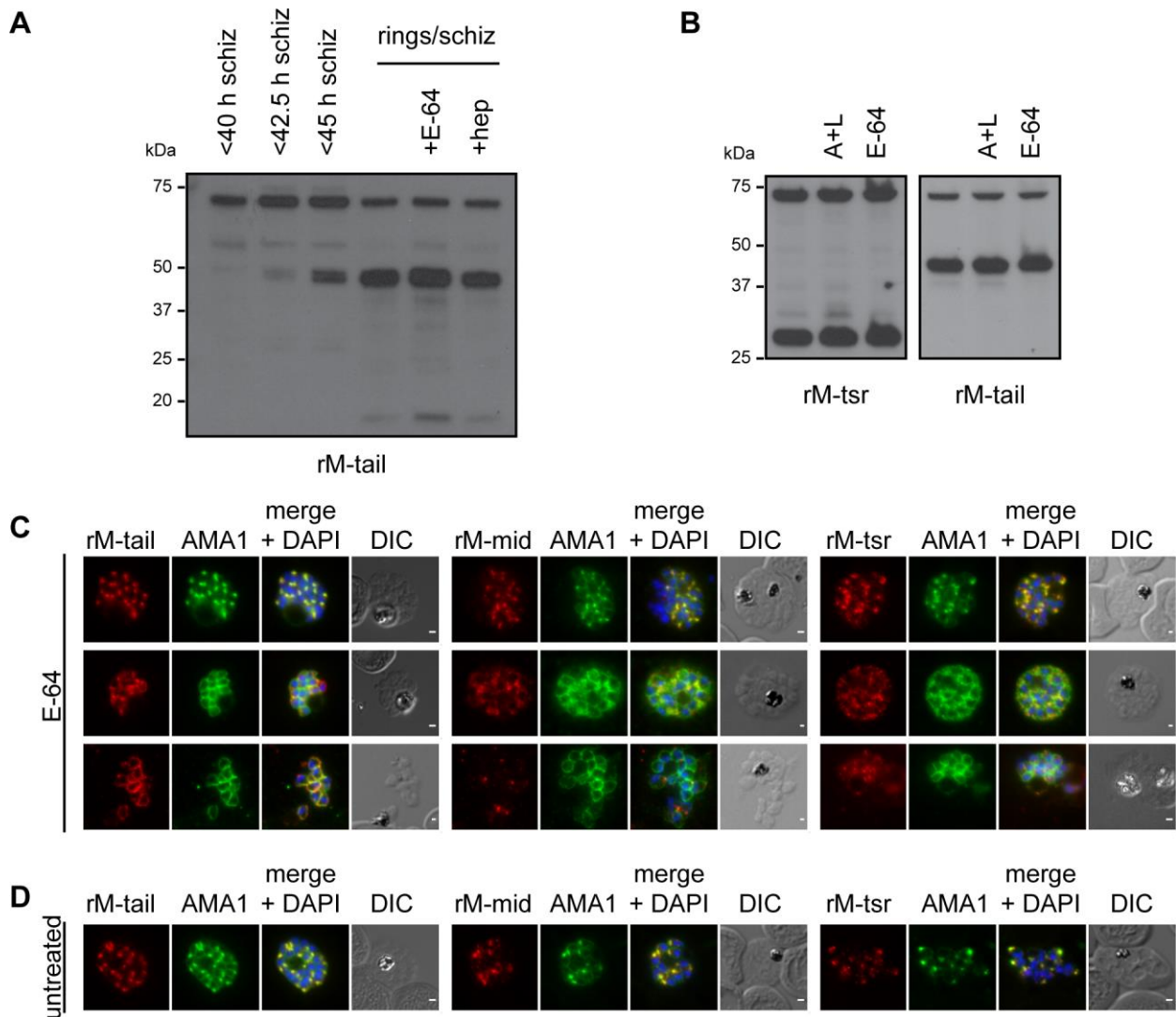


**Figure 6. MTRAP is cleaved irrespective of both invasion and egress from the schizont. A)** Immuno-blot analysis of a time course of tightly synchronised schizonts and early ring samples grown in the presence or absence of inhibitors of egress, E-64, or invasion, heparin (hep). Labelling with anti MTRAP tail (rM-tail) antibodies labels full length (~75 kDa) and cleavage products (~38/44 kDa) including the tail stub (~15 kDa). **B)** Immuno-blot analysis of tightly synchronised late schizont/early ring stage parasites grown in the presence or absence of inhibitors of egress, antipain and leupeptin (A+L) or E-64. Labelling with anti MTRAP tsr domain (rM-tsr) antisera identifies full length (~75 kDa) and cleaved tsr domain (~25 kDa). rM-tail labelling identified products as described above. IFA of very late stage schizonts **C)** treated with E-64 to prevent egress or **D)** from untreated culture, co-labelled AMA1 monoclonal antibodies (green) and rM-tail (left), rM-mid (middle) or rM-tsr (right) (red in respective images). Scale bars = 1  $\mu$ m.

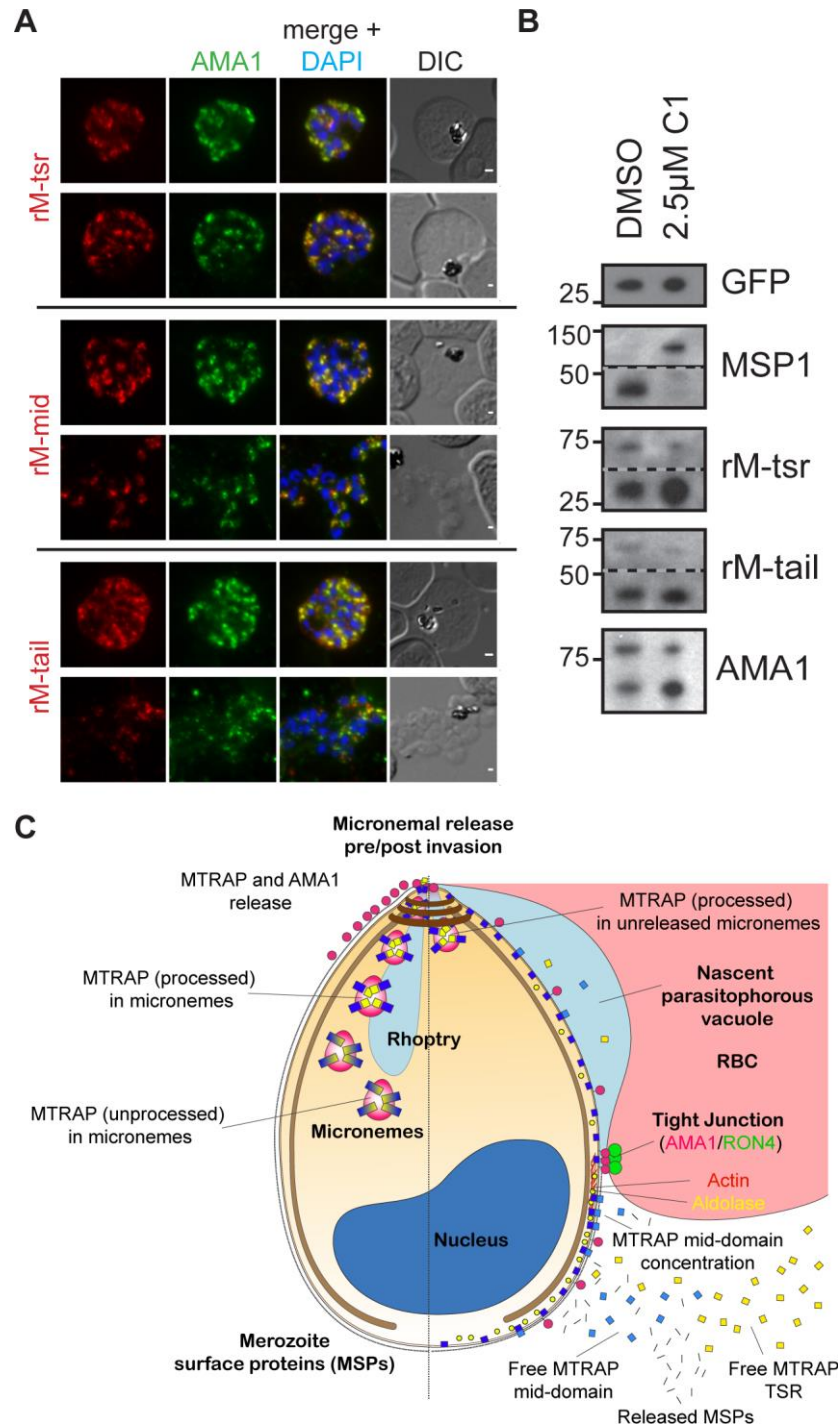


**Figure 7. MTRAP is cleaved within the micronemes.** **A**) IFA of compound 1 (C1) treated schizonts co-labelled with mAMA1 antibodies (green) and rM-tsr (top panels), rM-mid (middle panels) or rM-tail (bottom panels) (red in respective images). Scale bars = 1  $\mu$ m. **B**) Immuno-blot analysis of tightly synchronized late stage schizont/early ring parasites labelling for GFP (loading control), MSP1 (C1 treatment control), rM-TSR, rM-tail and rAMA1. **C**) Schematic of pre- (left half) and post- (right half) invasion merozoites, showing the predominant distribution of each protein tested as part of this study. It should be noted that all proteins show a degree of variability in labelling distributions across merozoites imaged to an extent that is not possible to depict here.